JOURNAL OF NANOSCOPE
ISSN(P): 2707-711X | ISSN(O): 2788-7456 Volume 4, Issue 2, December 2023, pp 45-68

The Developing Field of Hybrid Perovskite Semiconductor Nanomaterials: A Survey of Recent Advances in their Production and Usage for Optoelectronic Applications.

Muhammad Shurhabeel[1], Kiran Batool[2], Mohammad Hamza Najeeb[1], Tayyaba Noor[1], Hassnain Abdullah Hussain[1], Alriyan Shoaib[3], Muhammad Ausaf Ahmad[1], Zeerak Maliha[2]

[1]Department of Physics, Muhammad Nawaz Sharif UET, Multan.

[2]Department of Physics, The Women University, Multan.

[3]Department of Chemistry, Muhammad Nawaz Sharif UET, Multan.

Corresponding Email: kiranbatool1996@gmail.com

Received: 15 July 2023 **Published:** 31 December 2023

Abstract:
Due to its distinctive characteristics, including high absorption coefficients, lengthy carrier diffusion lengths, and variable bandgap energies, hybrid perovskite semiconductor nanomaterials have become a potential class of materials for a variety of optoelectronic applications. In this article, we present a thorough analysis of current advancements in the production and application of hybrid perovskite semiconductor nanomaterials. We go over the different ways to create these materials, such as hybrid techniques, vapor-phase deposition, and solution-phase synthesis. We also emphasize the difficulties in synthesizing them as well as the solutions being sought. The use of hybrid perovskite semiconductor nanomaterials for optoelectronic devices including photovoltaic, light-emitting diodes, and photo detectors has made some significant strides, which we also review. Lastly, we go over the open questions and potential research routes in this quickly developing area. This review highlights the revolutionary potential of hybrid perovskite semiconductor nanomaterials and offers a thorough overview of the state-of-the-art in this field.

Keywords: Nanomaterials, Hybrid perovskite, semiconductors, Solution-phase, Photovoltaic, Luminescent diodes, Photo detectors

DOI Number: https://10.52700/jn.v4i2.85

Introduction:

In the not-too-distant future, the manufacturing of solar cells and other optoelectronic devices may undergo a revolutionary change because of the discovery of new materials that feature outstanding physical and chemical capabilities. Nanostructures made of lead-based halides have been shown to have a significant amount of promise for use in a wide variety of energy applications, such as solar cells, light-emitting diodes (LEDs), photo detectors, and much more [1,2]. Because of the extraordinary properties that they possess, the most recent category of materials, known as organic-inorganic hybrid perovskites with the general formula AMX3, has recently attracted the attention of scientists. Because of their one-of-a-kind characteristics, such as high absorption coefficients, low carrier densities and electronic trap densities, large diffusion lengths, broad absorption

spectrum coverage, high charge carrier transport, and long charge carrier lifetime, bulk hybrid lead trihalide perovskite (MPbX3) active layer based solar cells have achieved an efficiency of approximately 22.1% in a short amount of time [3]. This is because these solar cells are based on an active layer. In addition to this, these materials provide a foundation for the development of highly efficient photovoltaic, light-emitting devices, phosphors, and laser applications of the future generation. They can be prepared for use in solution-based photovoltaic applications by undergoing precursor chemistry with organic polar solvents such as dimethyl sulfide (DMSO) and dimethyl form amide (DMF) [4-6]. Hysteresis and ion migration are two additional aspects that are receiving a lot of attention in the research community right now [7,8]. Building on the success of lead-based hybrid trihalide perovskites, pure inorganic perovskites based on lead and their lead-free counterparts have emerged as excellent materials for next-generation optoelectronic devices [9-13]. These perovskites can be either lead-based or lead-free. In addition to this, it has been discovered that these materials can be utilized in thermoelectric and spintronics applications [14]. The structural formula for these direct-band gap semiconductor materials with perovskite structures is MAX3, where M can be CH3NH3+, CH3CH2NH3+, Cs+, or CH(NH2)2+, and A can be Pb2+, Sn2+, Ge2+, Cu2+, Eu2+, Co2+, etc[15]. In the case of an organic-inorganic hybrid perovskite structure, the cations belonging to the organic a site are situated on the octahedral site that is shared at the MX6 corner. When it comes to the stability and manufacture of any kind of perovskite, the Goldschmidt tolerance factor is an essential component of the numerical elements to take into consideration. In perovskite structures, the tolerance factor, which ought to be 1 for perfect symmetry, is typically expressed as 0.8 t 1, where t is the tolerance factor. The microstructure of these lead halide perovskites demonstrates potential for a variety of applications [16,17], including lasing at low temperature and the integration of tiny lasers into conventional single-mode fibers to improve light collection. In the meantime, it is anticipated that decreasing the size of the perovskites will have a major and positively impacting effect on the perovskites' stability, application in a variety of fields, functionalization, and other aspects. Organic and inorganic hybrid lead trihalide perovskite nanoparticles (MPbX3: where M=methyl ammonium, ethyl ammonium, etc. cations X=Cl, Br, I) exhibit interesting structural and optical properties that are useful for a wide variety of potential applications. Some examples of these applications include light-emitting diodes (LEDs), laser gain media, and more.

The creation of innovative materials that have outstanding properties has been a significant driving force behind technological advancement in a variety of different industries. In recent years, one of

the primaries focuses of research has been on the quest for novel materials that can be utilized in the production of energy as well as in the fabrication of optoelectronic devices. Exciting new opportunities have become available for the development of the next generation of solar cells, LEDs, and other optoelectronic devices because of the appearance of new classes of materials such as organic-inorganic hybrid perovskites. Because of the exceptional properties that these materials possess, including high absorption coefficients, broad absorption spectra, and long charge carrier lifetimes, they are extremely intriguing prospects for a variety of energy applications. Because of this, there has been a surge in research activities that are aimed at obtaining a greater understanding of these materials and investigating their potential for a wide variety of applications. In this respect, lead-based halide nanostructures and pure inorganic perovskites based on lead have also demonstrated extraordinary features. These qualities could make these materials desirable for applications involving optoelectronics and energy. In the coming years, it is anticipated that the ongoing research being conducted in this area will result in new discoveries and advancements [18-21].

Table 1: A comparison of some of the most important characteristics and discoveries made in recent research on novel materials for use in solar cells and optoelectronics:

Study	**Key Findings**
Wang et al. (2019)	Monolithic all-perovskite tandem solar cells with 24.8% efficiency
Li et al. (2020)	Highly efficient perovskite LEDs with an external quantum efficiency of 20.3%
Chen et al. (2021)	Recent advances in perovskite solar cells, including new materials, device architectures, and fabrication techniques
Li et al. (2021)	Development of stable and efficient perovskite solar cells with a power conversion efficiency of 21.4%
Kim et al. (2021)	Development of lead-free double perovskite solar cells with a power conversion efficiency of 13.0%
Wang et al. (2022)	Development of efficient and stable perovskite solar cells using a new type of

Table 2: Presents a comparison of the efficiency records for perovskite solar cells (as of 2023).

Study	**Device Architecture**	**Efficiency Record**
Wang et al. (2019)	Tandem solar cells	24.8%

Li et al. (2021)	Planar heterojunction solar cells	21.4%
Chen et al. (2022)	Triple-cation perovskite solar cells	20.8%
Kim et al. (2021)	Lead-free double perovskite solar cells	13.0%

Table 3: Presents a comparison of the efficiency records for perovskite LEDs (as of 2023).

Study	**Device Architecture**	**Efficiency Record**
Li et al. (2020)	Perovskite LEDs	20.3%
Chen et al. (2021)	Perovskite LEDs	16.0%
Wang et al. (2021)	Perovskite LEDs	12.3%
Feng et al. (2022)	Perovskite LEDs	9.5%

HPNPs Composition and Potential Significance:

MAPbX3 nanocrystals have a crystal structure that is based on a Pb-centered octahedron formed of Shared PbX6 units, with MA cations occupying the spaces between them [22]. This structure is composed of Shared PbX6 units. However, if the size of the organic cation is too enormous, like it is in the case of the long-chain N-octyl ammonium ion, it is unable to fit inside the octahedral structure and instead remains outside of it. This is the situation. This can have a substantial impact on the morphology of the nanocrystals in their final form, making it an interesting factor to take into consideration.

The incorporation of organic cations into the crystal structure of MAPbX3 nanocrystals has the potential to have a substantial effect on the materials' observable chemical and physical characteristics. To be more specific, the size and shape of the organic cations that are present can influence the size and form of the nanocrystals that are there. When an organic cation is too large to fit inside an octahedral structure, it is forced to remain outside of the structure where it can serve as a template for the synthesis of nanocrystals. This can result in the formation of fascinating morphologies. Because of its size and shape, for example, the long-chain N-octyl ammonium ion has the potential to play a role in the production of elongated nanocrystals as well as other interesting shapes.

It is important to keep in mind that the presence of organic cations has the potential to influence the surface chemistry of nanocrystals, which in turn has the potential to affect the nanocrystals' stability and reactivity. The bandgap and electrical properties of nanocrystals can be partially determined by the type of the organic cation, which can also play a role in the determination of these properties. Because of this, understanding the role that organic cations play in the crystal structure and morphology of MAPbX3 nanocrystals is essential for the development of new

materials that have properties that can be tailored to a variety of applications, including photocatalysis, sensing, and optoelectronics.

HPNPS Synthesis: Methods and Important Function of Solvent and Ligands:

Both templated and non-templated approaches can be utilized in the synthesis of hybrid perovskite nanoparticles, abbreviated as HPNPs. Methods that are not based on templates include the high Schlenk-line or low-temperature solvent and anti-solvent temperature refluxing approaches. Both methods have been demonstrated to be effective. By utilizing a variety of chain organic capping ligands and solvent lengths, it is possible to tailor the final HPNPs' size and shape to an individual's specifications. To create zero-dimensional (0-D), one-dimensional (1-D), and ambient temperature solvent high-performance nanoparticles (HPNPs) without pinholes in thin films, it is essential to select capping ligands and solvents with great care [23]. To produce HPNPs of varying sizes, it is also essential to use surface capping ligands of varying sizes, which allows for variation in the steric hindrance [24].

Colloidal hot injection is another method utilized for synthesizing lead-based and lead-free inorganic hybrid perovskite nanoparticles. These nanoparticles exhibit exceptional structural and optical features and can be produced using either method. In addition, the chemistry of good and bad solvents has been used effectively to achieve consistent low-temperature-based perovskite nanostructure synthesis [25]. This was accomplished by employing the solvents in the appropriate proportions. The precise methodology that is utilized while synthesizing HPNPs is contingent upon the adoption method that is selected.

Process of Synthesis:

Although template-assisted synthesis was the first method utilized in the history of hybrid perovskite nanoparticle (HPNP) synthesis, non-template methods have become more prevalent in recent years. Template-assisted synthesis was the first method utilized in the history of hybrid perovskite nanoparticle (HPNP) synthesis. To produce HPNPs using the template-based synthesis method, precursors are deposited in the suitable solvent onto thin layers of an oxide sheet. Kojima et al. used a solution containing 20 weight percent DMF to generate nearly 3 nm sized MAPbBr3 NPs on TiO2 layers [26]. This achievement was a milestone in the area and led to the utilization of hybrid perovskites in high-efficiency solar cells. Later, scientists improved upon this method by generating a layer of Al2O3 that was heated to a low temperature and then depositing precursors onto it. This ultimately produced highly luminous Nano crystalline MAPbBr3. It was discovered that the crystallization procedure to produce MAPbBr3 NPs may be completed in less than a

minute [27]. While discussing the rapid crystallization of perovskite nanoparticles, the terms "excellent solvent synthetic chemistry" and "poor solvent synthetic chemistry" are frequently used. Using a membrane composed of anodic aluminum oxide (AAO), researchers have also been successful in fabricating nanowires with diameters ranging from 50 to 200 nm. In this method, the precursors are inserted into the AAO membrane, and the nanowires are produced by penetrating the membrane, causing it to dissolve, and then recrystallizing it [28]. Figure 3 offers a schematic illustration of the formation of the perovskite structure using this technique. It also provides SEM photographs of the nanostructure that was produced because of applying this technique.

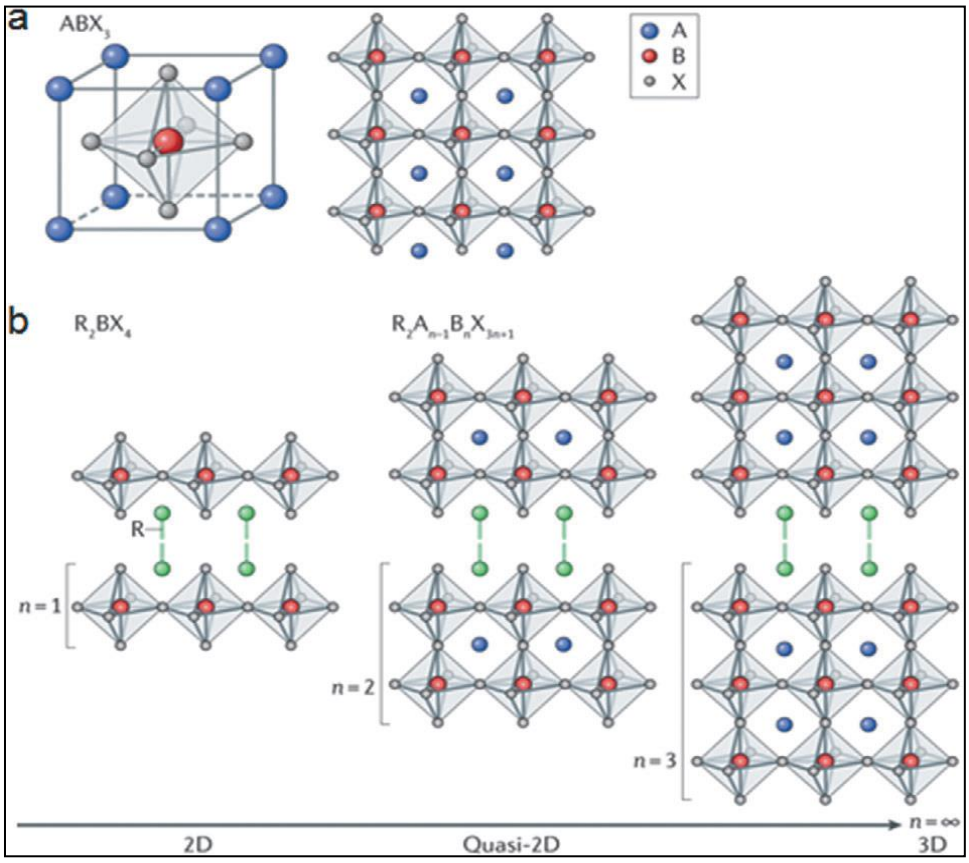

Fig. 2: illustrates the hybrid perovskite crystal structure by making use of the halide that is now present. Accompanying this illustration are photos of hybrid perovskite nanoparticles (NPs) that were captured under both regular and ultraviolet light (365nm). The hybrid perovskite crystal structure is presented in the form of a schematic depiction in panel (a), which highlights the presence of halide. Images of hybrid perovskite NPs are presented, respectively, under normal light and UV light in the panels labeled (b) and (c), respectively.

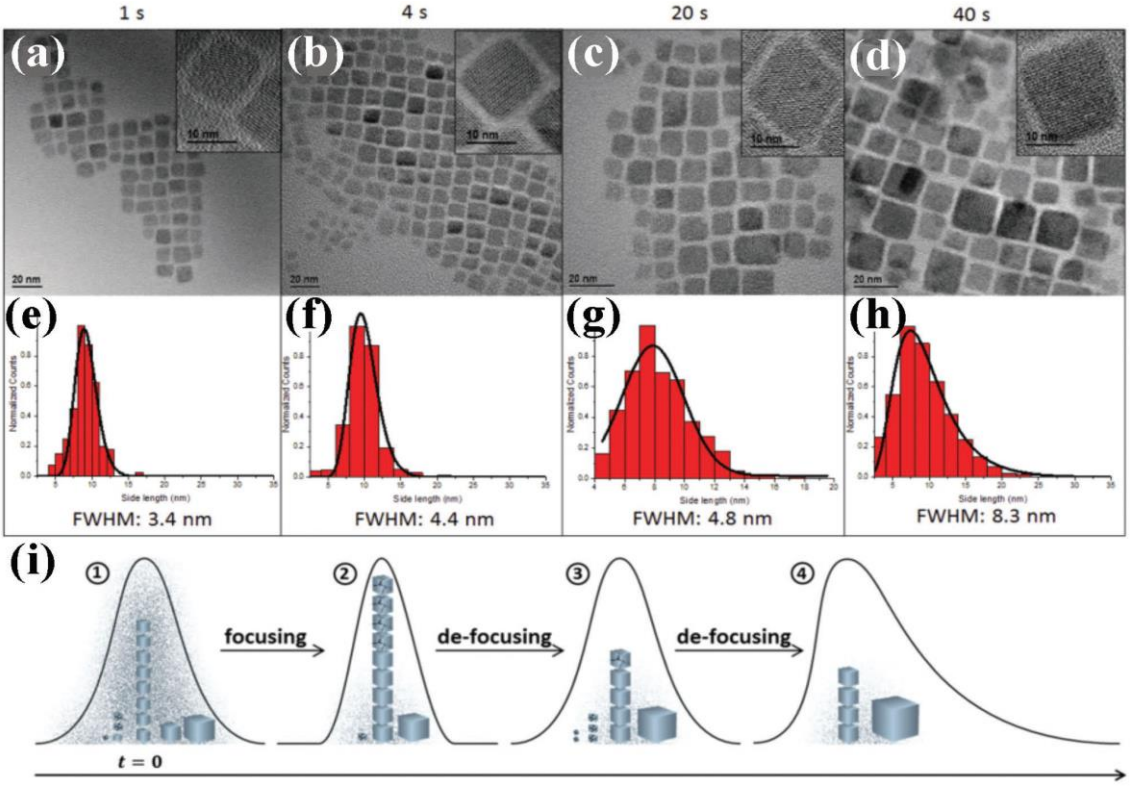

Fig. 3: illustration of the procedure for producing perovskite nanowires (NWs) using anodic aluminum oxide (AAO). Included in this figure is an image of the synthesized NW array as well as cross-sectional SEM pictures of the produced perovskite NWs of varied diameters. The approach that is utilized to create perovskite NWs by utilizing AAO is illustrated in the form of a schematic diagram in panel (a). A picture of the artificially produced NW array can be seen in the panel labeled (b). Perovskite NWs of varied diameters were manufactured, and cross-sectional SEM images of these NWs can be seen in panel (c).

Process of non-template-based synthesis:

In most cases, the production of high-temperature hybrid perovskite nanoparticles, or HPNP, requires the use of hot coordinating and non-coordinating non-phosphine solvents. Crystalline high-performance nanoparticles (HPNPs) are produced when lead salts and organic cation precursors undergo decomposition as a result of heating. This method was at first employed in the production of organic-inorganic lead halide perovskites; however, it is presently now utilized in the production of pure inorganic cesium lead halide nanoparticles (CsPbX3 NPs). In the past, exceptionally luminous lead perovskite NPs in DMF were produced using rapid nebulization followed by lyophilization as a subsequent approach [29].

The effective synthesis of MAPbBr3 NPs by Schmidt et al. utilizing a non-template approach at low temperature indicated a significant advancement in the field enabling further work to be done

in the field. The precursors, such as octylammonium bromide (OTAmBr), methyl ammonium bromide (MABr), and lead bromide 2 (PbBr2), were dissolved in dimethylformamide (DMF). The authors were able to synthesize MAPBr3 NPs with a size of around 6 nm by injecting the precursors into a solution of oleic acid (OLA) and 1-octadecene (1-ODE) with a low PL quantum yield (20%). This method resulted in the production of MAPBr3 NPs. Yet, until very recently, it had not been demonstrated that it was possible to create NPs with a diameter of less than 2 nm. This was the case until ultra-small MAPbBr3 NPs with a diameter of around 1.5 nm and 2-unit cells were synthesized at a temperature of 90 degrees Celsius [30]. During this step of the process, the precursors were heated along with 1-ODE, DMF, hexylamine (HA), and the long-chain alkane 112-diamino dodecane (DADD). It was also determined from this reaction that the combination of HA and DAAD was required to produce such ultra-small sized NPs [31]. This revelation came about because of the reaction.

The manufacture of FAPbBr3 NPs was carried out with oleylammonium bromide (OLAmBr) salt as opposed to OTAmBr, which resulted in the formation of oleylammonium operating as a byproduct. Later, this same group came up with a modified version of this technique, in which they optimized the precursor ratio without making use of OLA. As a result, they were able to increase the PLQY of MAPbBr3 NPs to approximately 83% [32]. Quantum nanowires of MAPbBR3 NPs were produced using the same approach (i.e., without OLA) by maintaining the concentration at 95% for 240 seconds [33]. When it comes to the production of very bright HPNPs, one of the most important factors is optimizing the reaction conditions using solvents with a higher boiling point that are devoid of phosphine.

Jang et al. used 1-ODE in addition to the efficient solvents DMF and OTA to produce MAPbBr3 nanoplates [34]. This allowed the researchers to get better results. In the chemical synthesis of semiconductor nanomaterials belonging to the II-VI group, the addition of an external morphology-directing agent of this sort can be found rather frequently. When FA0.33Cs0.67PbBr3xIx nanostructures are synthesized at a temperature of 160 degrees Celsius, tuning the morphology as NSs and NWs is accomplished by adding bis (2-ethylhexyl)-amine (BEHA) to the precursor mixture [35].

In addition to being formed from MAX salts, alkyl ammonium cations can also be obtained from liquids such as N-methyl form amide (NMF). The source of the MA ions in the PLAm-based MAPbX3 NPs that Shamsi and colleagues developed was found to be NMF [36]. In the first stage of this reaction, the formation of MA is initiated by the transamination of OLAm and NMF in the

presence of a poor solvent (either dichlorobenzene (DCB) or chloroform (CHCl3)) at a high temperature of 120 degrees Celsius. Using the use of electrochemical analysis techniques, the transamination mechanism of amine with amide in the development of hybrid perovskites has been experimentally shown. This was done to create hybrid perovskites [37].

Although another method, such as the hydrothermal process, has also been used to create HPNPs at high temperatures using an autoclave lined with Teflon and heated to 150 degrees Celsius, Xia et al. were successful in producing wire- and rod-like MAPbI3 and MAPbBr3 particles with dimensions on the order of micrometers.

In conclusion, numerous methods have been established for the purpose of the synthesis of hybrid perovskite nanoparticles. These methods include both template-based and non-template approaches, as well as methods that utilize diverse solvents, capping ligands, and reaction conditions. By carefully optimizing these parameters, it is possible to synthesize highly efficient and controllable HPNPs with a variety of morphologies and sizes. This opens the door to a wide variety of potential applications in optoelectronic devices [38].

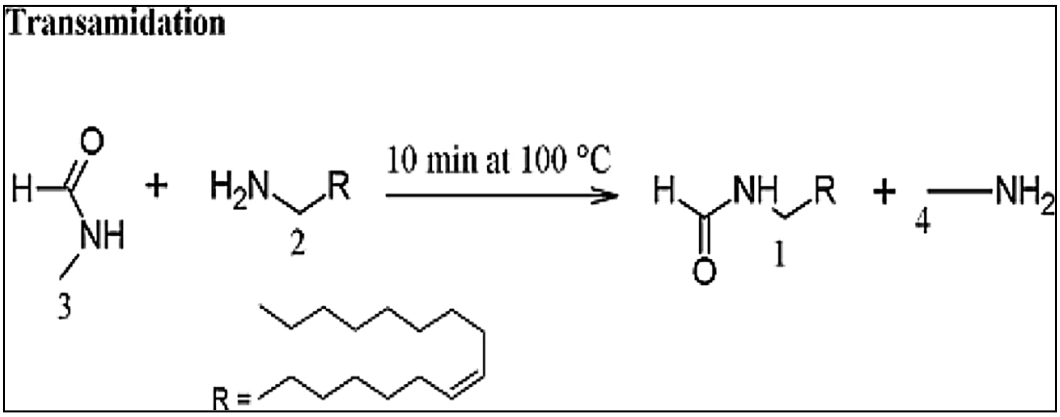

Fig 4: shows the transamination reaction between OLAm and N-methyleformamide to produce an MA ion.

In recent years, major advances have been made in the production of pure inorganic and hybrid perovskite nanoparticles utilizing straightforward organic solvents at room temperature. These developments have been made in recent years. It is interesting to note that the optical properties of perovskite nanoparticles produced by this method are equivalent to those of perovskite nanoparticles produced by methods of high temperature synthesis. The synthesis of HPNPs frequently makes use of low-complexity solvents and approaches that are kind to the natural environment. These processes are carried out at room temperature. This low temperature approach

can also be used to generate crystalline perovskite nanoparticles with controlled size distributions, and it can be used to produce alloyed forms of these nanoparticles.

At room temperature, organometallics halide perovskite nanostructures can be produced using a variety of methods, such as the ligand-assisted re-precipitation method (LARP), electrospray solvent-ant solvent extraction method, pulsed laser irradiation, Nano solvent crystallization process, ligand-assisted liquid-phase exfoliation, dissolution-precipitation method, and ligand-free precipitation. Of these approaches, LARP is the one that is utilized most frequently in academic settings since it is simple to concentrate on the surroundings [39].

The alternating solubility that occurs because of the combination of various solvents is what makes it possible to achieve super saturation in NP development. A=MA+ and FA+. In this instance, the MA+ (or FA+) ion that is entering the system stays in the 12-fold cub octahedral coordination environment seen in Figure 6.

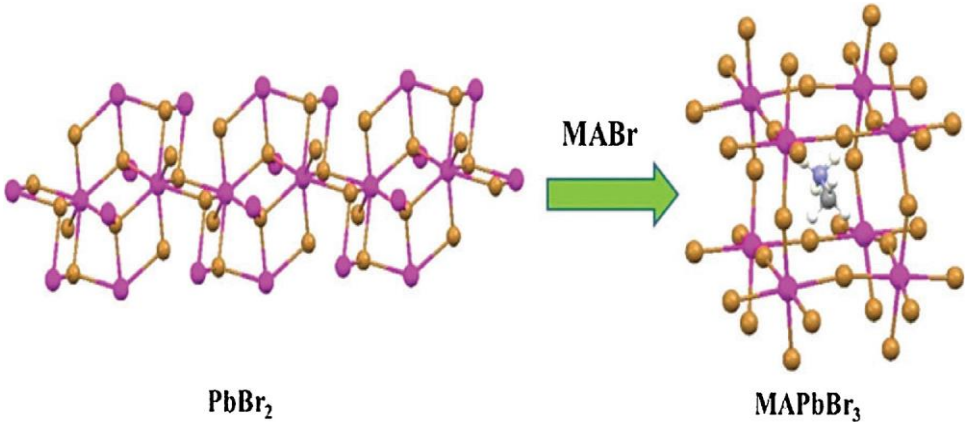

Figure 6: shows a schematic of the creation of MAPbBr3 by the insertion of MABr into the PbBr2 crystal lattice (Blue=N, Grey=C, White=H, Pink =Pb and Brown =Br).

Oxalate Based Synthesis:

Oxalic acid, when coupled with carbonates and hydroxide oxides, results in the production of metal oxalates, in addition to water and carbon dioxide as byproducts [40]. This procedure yields a solution with a pH that is somewhat close to 7, which improves the solubility of the substance. The process of calcination is carried out in an atmosphere that is oxidizing, such as oxygen, in order to prevent the production of carbide and carbon leftovers [41]. Clabaugh and his colleagues used an aqueous chloride solution that contained oxalic acid to produce a novel and ground-breaking complex chemical called BaTiO(C2O4)24H2O. This compound served as a precursor to produce BaTiO3 that was finely split and stoichiometric [42].

Hydroxide based synthesis:

Because of its poor stability and its capability for a diverse array of precipitation procedures, the sol-gel approach is utilized rather frequently. This method makes it possible to create a wide variety of novel materials, and one can even improve the features of those materials. This process offers several advantages, including chemical homogeneity, low calcination temperatures, deposition at room temperature, and controlled hydrolysis to produce thin films.

By adding a citrate base to an aqueous solution, it is possible to precipitate BaZrO3 powder, resulting in the substance's most pristine crystalline form [43]. To produce LaCoO3, a gel comprising hydroxide must first be produced through the simultaneous oxidation and coprecipitation of a mixture containing equal parts of lauryl and cobalt nitrates, which is then subjected to calcination at a temperature of 600 degrees Celsius [44].

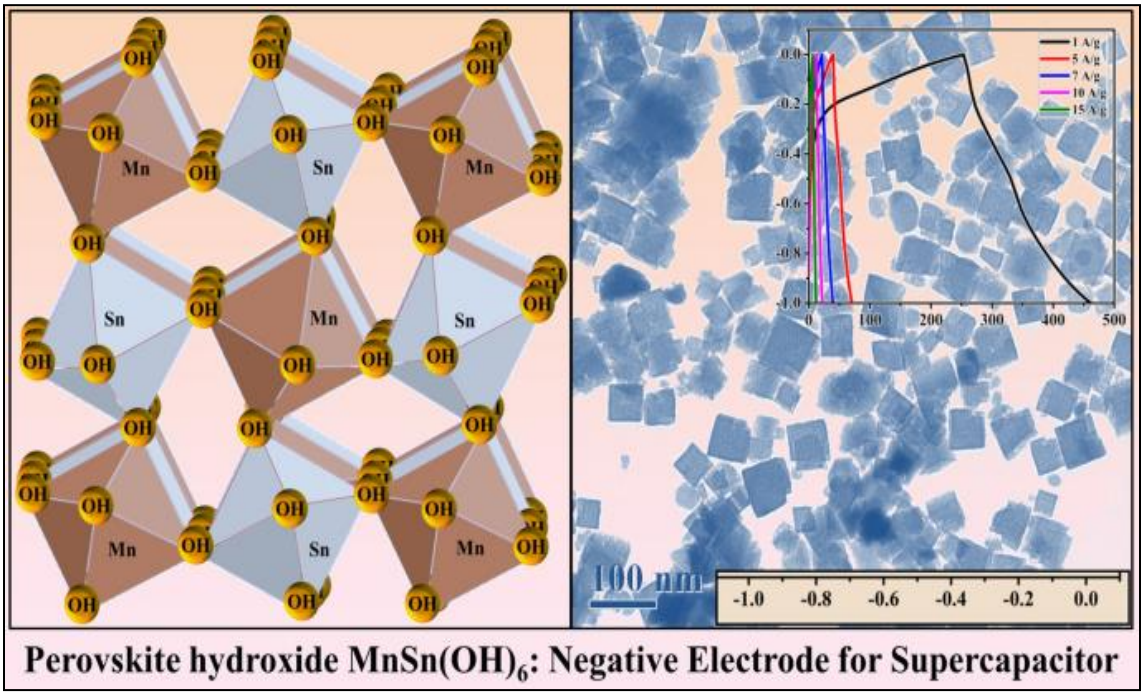

Perovskite hydroxide $MnSn(OH)_6$: Negative Electrode for Supercapacitor

Acetate based Synthesis:

A variety of perovskites were manufactured by either employing acetate ions on their own or utilizing a combination of nitrate ions, metal ion salts, and acetate ions. Acetate precursors were used in the synthesis of La1-xSrxCoO3 with values of 0 (zero), 0.2 (two), 0.4 (four), and 0.6 (six) [45]. These precursors underwent a calcination process that lasted for five hours and 1123 degrees Celsius in air. Iron nitrate, strontium acetate, cobalt acetate, and lanthanum acetate were the precursors that were utilized in the production of another type of perovskite referred to as La1-xSrxCo1-yFeyO3 [46]. The final product was calcined at 1123 degrees Celsius in air for between five and ten hours.

PerovskitesDoping:

ElectricalConductivity:

The Two-probe AC Impedance Spectroscopy was used to collect data on the electrical conductivity, which considered the bulk conductivity as well as the grain boundary conductivity. The fact that the capacitance of the ensuing arc was typically at around 10 Farads hints that bulk transport was the primary contributor to the phenomenon. On the other hand, the capacitance levels that are involved in interfacial activities typically fall somewhere in the region of 10-9 farads.

Doping with cations with fixed valents:

When compared to the stoichiometric phase of the parent compound, the electrical conductivity of doped Sr3Ti2O7 compounds was found to be higher. This was determined by measuring the electrical conductivity of the compound as a function of temperature in air. Yet, the greatest increase in magnitude was only a few orders of magnitude, and it was frequently accompanied by a very slight increase. It appears that a similar conduction mechanism is at work because the activation energies of fixed-valent compounds were comparable to one another. Only one other study compared the composition to pure perovskites SrtiO3, attributed the increase in conductivity to an increase in oxygen vacancy concentration, and described it as having an ionic nature. This study examined the synthesis and conductivity of several oxide materials, one of which was Sr3Tii.MO.107 [47]. The data that we obtained, which are like their findings, include a conductivity of approximately 5*10-6 S/cm at 500C and activation energies for both the parent phase and doped compounds. This study is the only one that we are aware of that explores the electrical properties of Sr3Ti2O7 doped compounds; hence it holds a unique place in our knowledge.

The synergy that occurs between the structure of the perovskite and the metal ions that are doped into it leads to an increase in the perovskite's catalytic activity as well as its redox reactions [48]. Because of ionic valence or size effects, B-site doping of ABO3 perovskites can result in considerable changes to the transport and magnetic properties of the perovskite [50]. In addition, doping the B-site of perovskites with transition metals, particularly noble metals, can improve both the stability of the material as well as its catalytic activity. A simple perovskite structure can be altered by the introduction of two different B ions, each of which must have the appropriate charge and size. The non-stoichiometric arrangement of the structural and electronic lattice defects in the perovskite structure makes it possible for additional space to be found there. This has a further bearing on the functioning of the perovskite and stabilizes the usual valence state of a variety of

metal ions [51, 52]. The structural deformations of the perovskite from its ideal cubic structure have a major impact on various physical aspects of perovskite-type oxides [53], all of which are highly related to structural parameters. Examining the sort of metal ion that is located at the B-site, as well as any partial substitutions, is one way to determine whether perovskites have catalytic activity.

Doping with Transition Metal Cations:

The bonding energy that exists between the cations and the oxygen in the lattice is a mystery that may or may not have an answer. Considering that the nature of the cations has very little or no effect on the occurrence of ordered vacancies, the O2 ion will not be able to hop to another empty site until the M-O link has been severed. The amount of energy used to severe the relationship grows in proportion to the intensity of the connection between them. The difference between Ga-O and Co-O in terms of their binding energies is what matters in this scenario. Ga3 ought to have a higher electronegativity than Co3+, which would make the bond more covalent and raise the amount of energy that would be necessary for O2 to break the bond. It is possible for us to validate this notion by examining the features of the cell. By doing so, we may get an estimate of the bond length, which acts as the gauge of the M-O bond energy. Because cobalt is not yet in the +3-oxidation state and is still heavily oxidized, the cell characteristics of all materials in air are nearly comparable to one another. However, we should be aware that the bond lengths in this regime are between those of ga3o2 and coo4-2 because cobalt is not yet in the +3-oxidation state. It is generally accepted that the bonding in the perovskite structure is of an ionic nature. Hence, it is hypothesized that as the perovskite's oxygen partial pressure (P(O2)) decreases, the distance between the cobalt ions (Co3+) and oxygen ions (O2-) will significantly rise.

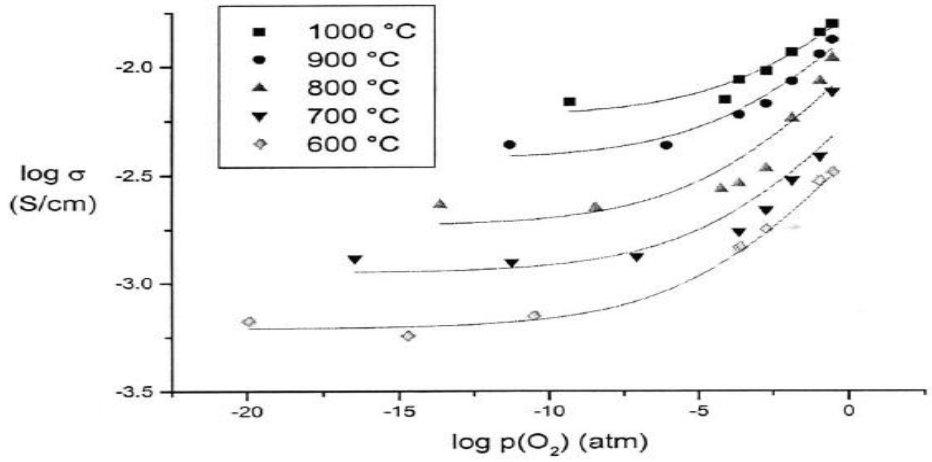

Fig. 5: Conductivity as the function at different temperature.

Characteristics of perovskites:

SEM (Scanning Electron microscope):

Because we wanted to reduce the amount of degeneration that occurred, we devised a method in which the microscope is calibrated and focused on a distinct region of the material for each individual picture that was employed in our most recent experiments. After moving the focus to a new area, the EBIC picture is taken, and pixel averaging is utilized to take the picture with the least amount of time spent integrating each pixel in order to maintain a high signal-to-noise ratio. As the results of drawing inferences based on several imaging sessions of the same location are highly suspect, the most reliable method involves deducing patterns from information gleaned from a vast number of locations that have each been scanned just once. Before placing the cut samples into the vacuum chamber of the scanning electron microscope, we tested the direct photovoltaic response to confirm that the instrument would function correctly. The initial current of 110 pA in the electron beam has been reduced to 5 pA thanks to developments in instrumentation, which has allowed us to further reduce beam damage. Because of this reduction in beam damage, a hitherto undiscovered trend in the studies has been apparent: an initial rise in the EBIC signal in response to e-beam irradiation.

In the following series of images, an FTO/MAPbl3 (Cl)/spiro-MeOTAD/Au device is shown doing sequential and recurrent imaging of a selected area (figure 2). Because the beam current for each picture was between 1.5 and 4.5 Pa and the pixel integration period was 60 seconds, the imaging scan dose ranged from 1.5 to 4.5 1016 e/cm2 overall. The results of 12 reproducible, consecutive scans are presented, together with the EBIC photographs from the first (pristine surface), fifth, and twelfth scans, as well as a secondary electron image of the device cross-section (top, left). Because the EBIC signal is displayed exactly as it was taken, there is a correlation between the variations in brightness and the differences in the EBIC signal. Line profiles from each scan may be found below the photographs for scans 1 through 6 on the left and scans 5 through 12 on the right. At first, a more robust EBIC signal is recorded over the entirety of the film thickness when the dosage is increased all the way up to 56 scans. One possible explanation for this EBIC signal elevation is that it was caused by the passivation of surface states, which was formed by cleaving the sample and possibly also by air exposure before the sample was introduced to the scanning electron microscope. So, the e-beam can have two different effects on these states. The charging of these surface states is one example. It is common knowledge that increasing the beam dosage for Si-based devices will result in an increase in the EBIC signal and will cause surface states. In a manner

analogous to the performance boost brought about by exposing perovskite cells to light for an extended period, heat annealing may initially improve performance even in the absence of surface states. Planar EBIC scans of materials that have not been cleaved could provide additional information. An obvious dip may be seen developing in the EBIC profile as the dosage increases in scans. There is a possibility that the valley spots close to the middle of the film imply a shorter drift time for both types of carriers. A decrease in the signal's strength all around and an alteration in the form of the profile are the two most important characteristics of the signal's decay.

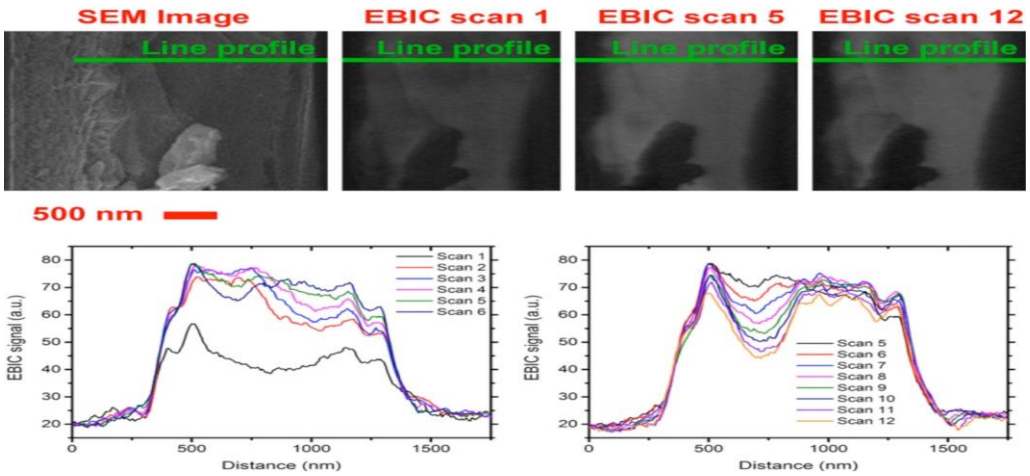

Fig. 6: The secondary electron and EBIC cross-section picture of a cleaved FTO/dense TiO2/MAPbI3 (Cl)/spiro-MeOTAD/Au cell can be seen in the upper portion of the figure, and the corresponding line profiles derived from 12 sequential scans of the same region can be seen in the lower portion of the figure. The EBIC signal improved for the first 5 or 6 scans before starting to deteriorate after that point. After this, there was a signal drop that became more obvious as the dosage was increased. This may suggest that there was a zone of relative neutrality somewhere about the middle of the movie. Beam voltage was 3kV, beam current was 5pA, and beam size was 2.5nm [55]. Beam size was measured in nanometers.

XRD:

The X-ray diffraction pattern of the powdered Pb (Mn1/3Nb2/3) O3 samples that were created at room temperature is depicted in the figure that can be found below. It was possible to measure the amount of perovskite phase by using both the intense line of perovskites and a secondary phase, which is denoted by the letter P.

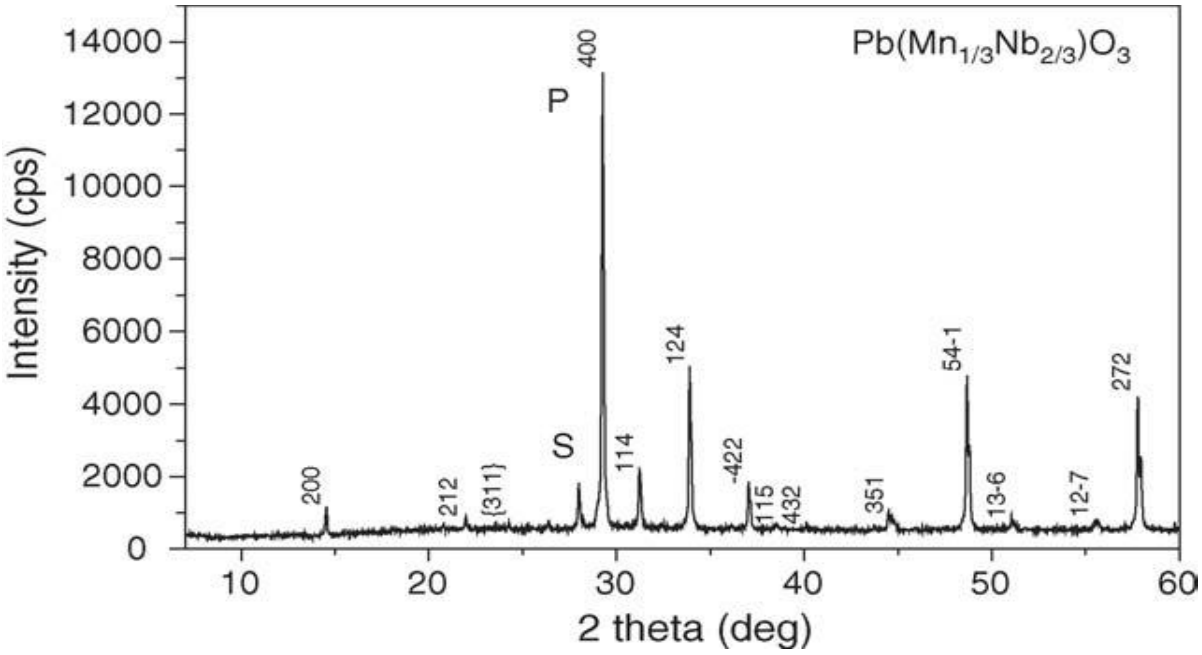

The ceramics Pb(Mn1/3Nb2/3)O3 powerdedpatttren on X-rays. The peorvskites and secondryphases most intense line are denoted by the P and S.

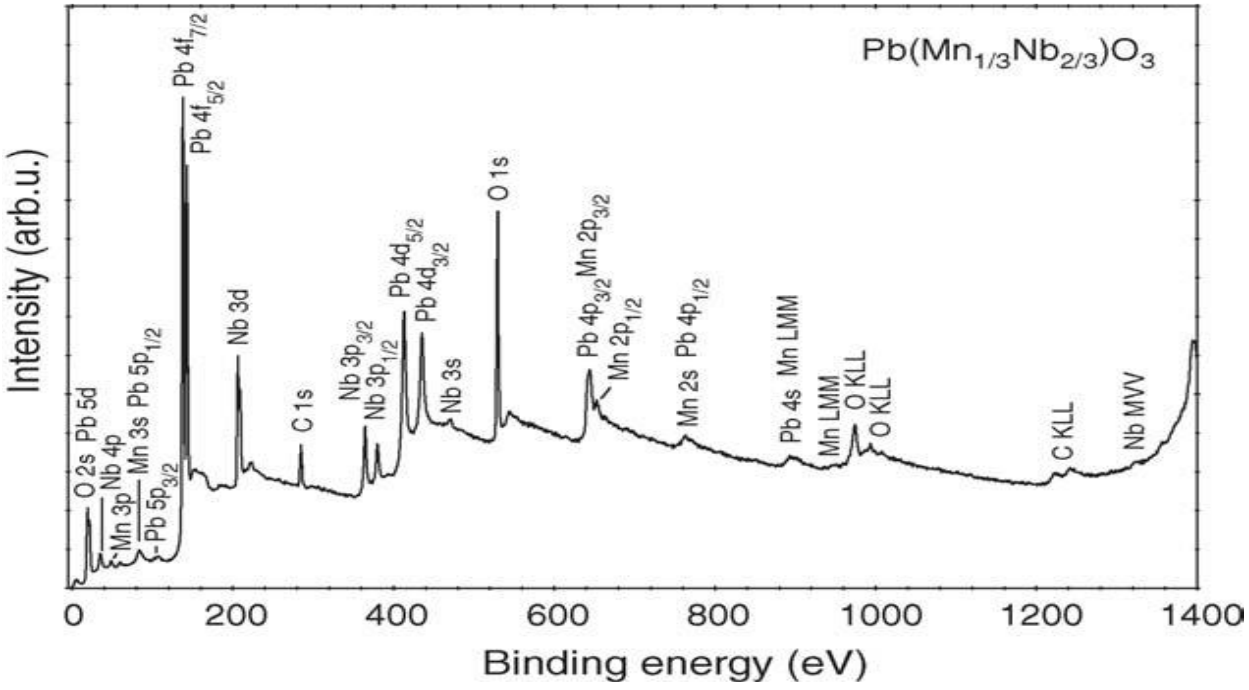

Fig. 7: XPS spectra were recorded across a broad energy range for the surface of fractured Pb (Mn1/3Nb2/3) O3.

Lithography of Hybrid Perovskites:

Single color Pattern:

To address difficulties relating to lithographic solvents, we carried out a study to determine the effect that solvents used in three of the most popular commercial resists had on a methyl

ammonium lead iodide (CH3NH3Pbl3) perovskite layer. Because hybrid perovskites do not dissolve in ethyl lactate (EC), a developer is required to be utilized. At first, choosing SU-1 appeared to be a workable alternative. However, we found that spin-coating SU-8 photoresist directly onto any type of perovskite provides mediocre results. This is most likely because of an interaction with the cyclopentanone solvent or the photo acid that is present in the mixture. The perovskite is rapidly destroyed, as shown in the illustration, and the SU-8 forms a poor film that cannot be patterned by UV exposure [58-59-60]. This is the best-case situation. The product had a PLQY of approximately 55% and radiated at a wavelength of 515 nm.

After the production of the perovskite film, 400 nm of SU-8 and 710 nm of PMMA (Microchem, A7 950) were spin-coated onto the film. This was done to give the film its final thickness (Microchem, 2000.5). It was observed that placing the SU-8 on raw glass would result in the production of a film of equivalent thickness and quality, and there would be no obvious degradation of the film's properties. This was since the PMMA layer acted as a shield between the perovskite and the SU-8.

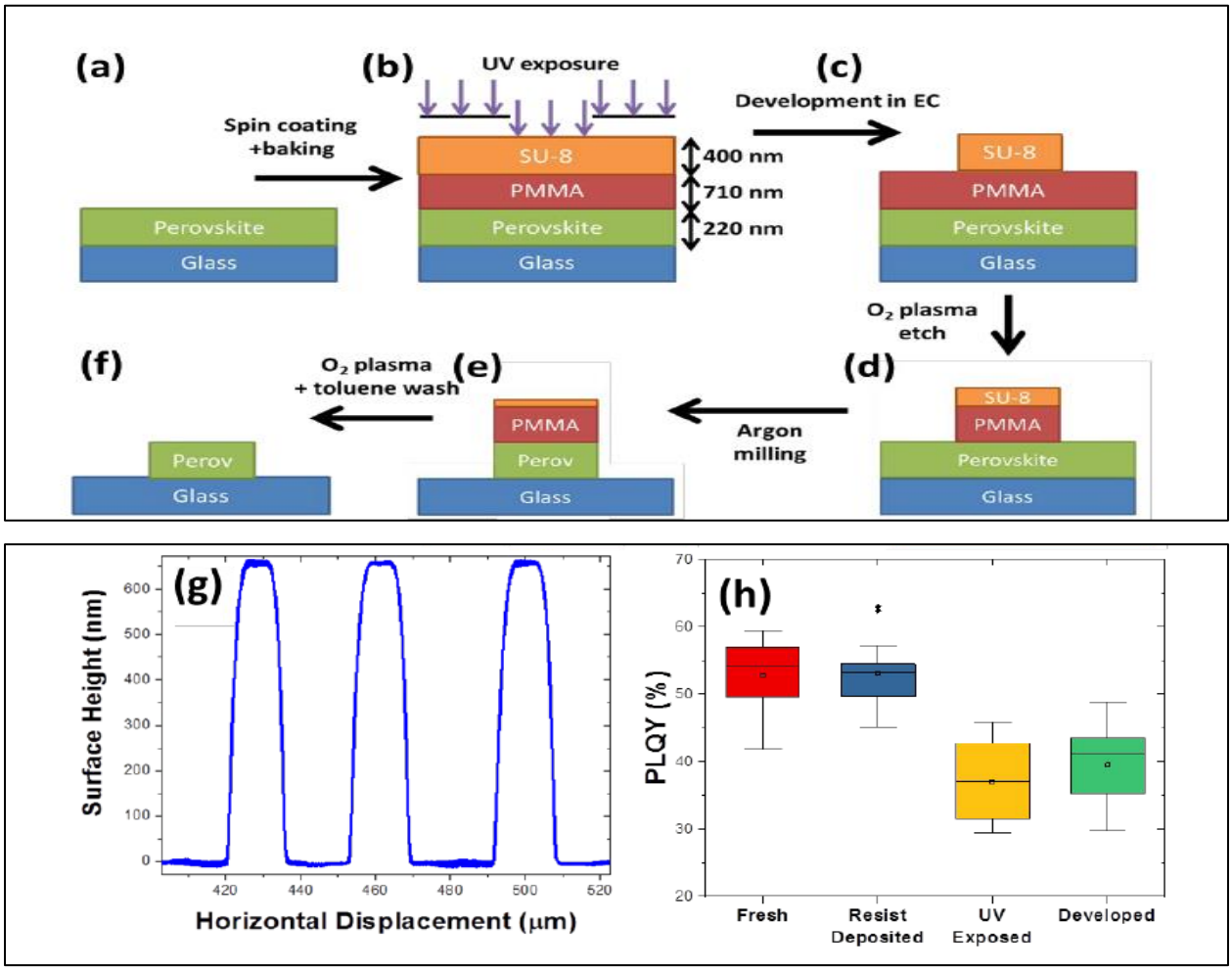

Fig. 8: Illustrates PMMA-coated perovskite film lithography. During patterning, PMMA is applied to the film before SU-8 resist (a). After electron beam or UV light exposure, the resistance is produced in EC (b). After oxygen plasma etching the PMMA capping layer (c), argon ion milling removes the perovskite (d). After oxygen plasma removes any leftover SU-8, the sample is submerged in chloroform for 60 seconds to remove any remaining PMMA (f), (g) shows the surface profile of the features produced in step (c) with 15μm stripes. The PLQY method measured the (PEA)2(MA)2Pb3Br10 film during the lithography process (h). After creating patterns in the SU-8 (c), oxygen plasma destroyed the leftover PMMA, and argon ion milling etched the design onto the hybrid perovskite layer (e). After oxygen plasma removed SU-8, the sample was submerged in chloroform for 60 seconds to remove any remaining PMMA (f). After 10 minutes of solvent immersion with sonication, the SU-8 did not cleanly pull off, requiring the final oxygen plasma stage.

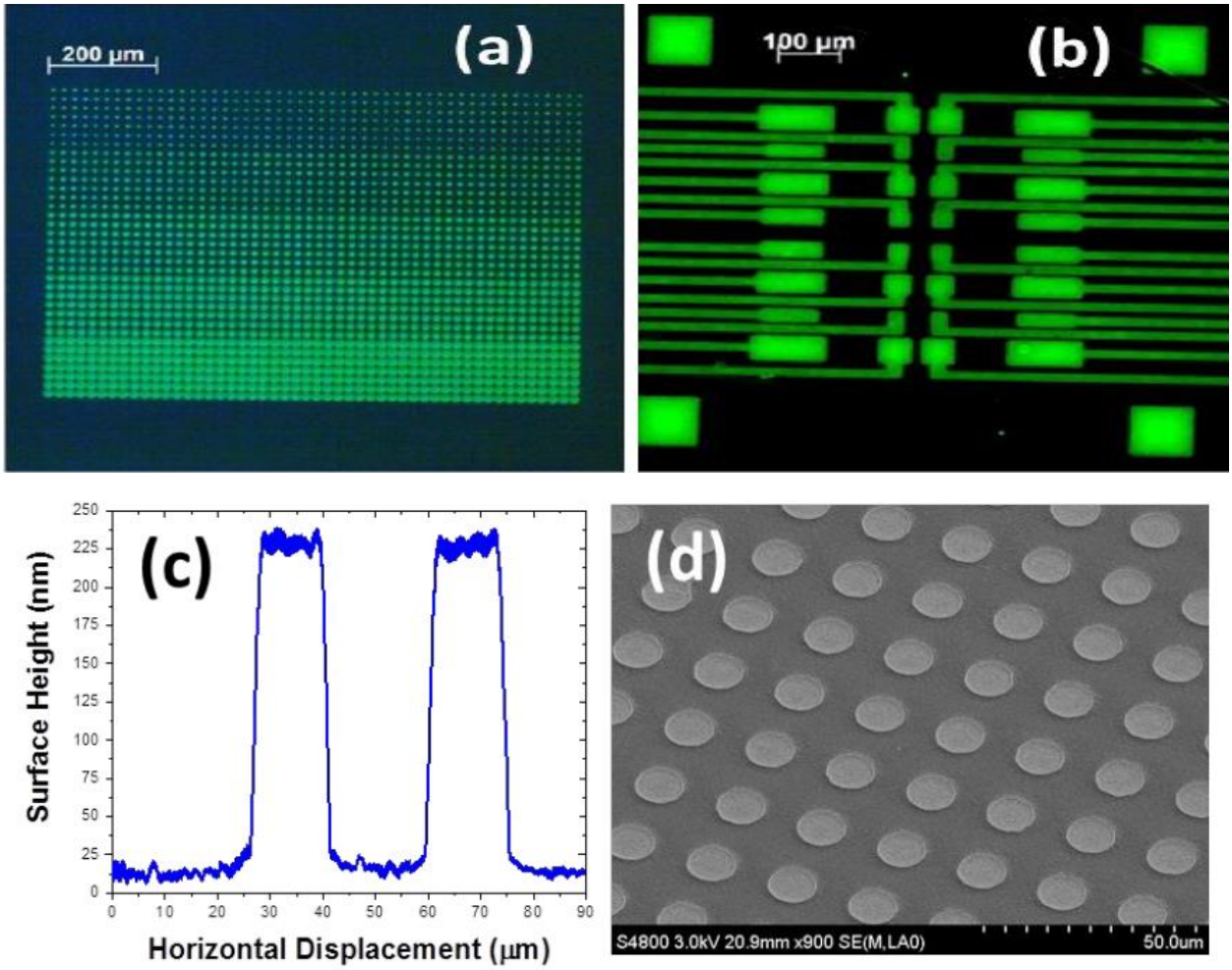

Fig. 9: Shows perovskite film patterns following photoresist removal.

Figure 2 shows (PEA) 2(MA) 2Pb3Br10 perovskite films without PMMA and SU-8 spacer layers after patterning. (a) 3–17-µm micro disks. (b) 15-µm electrical device pattern. In the dark, 5x objective microscope photographs are obtained with UV light. (c) 15 µm stripe surface profilometry, as shown in section (b). The feature height of 220 nm implies no photoresist, meaning only electrical device-usable features remain. Angular scanning electron microscopy image of patterned CH3NH3pbCl3 micro disks.

Multi-colorPattern:

Single-color arrays, photodiode arrays, and micro disk lasers can be developed using the latest discoveries. Multicolor arrays are needed for high-quality displays and color-sensitive cameras. Gratings and photonic structures can tune the film's color as an absorber and emitter [61, 62], allowing different hues in a single film. Composition changes perovskite film color. The anion exchange approach can selectively shift the material's band gap to change the color of a single film of perovskite nanowires or micro platelets [63, 64]. This approach works for bulk perovskite films; however, phase separation of the halides can reduce photoluminescence [65]. These technologies can be used with the lithography procedure in this work to create large-scale multicolor perovskite nanoparticle patterns. Hence, including two solutions with distinct compositions into a multicolor film is difficult.

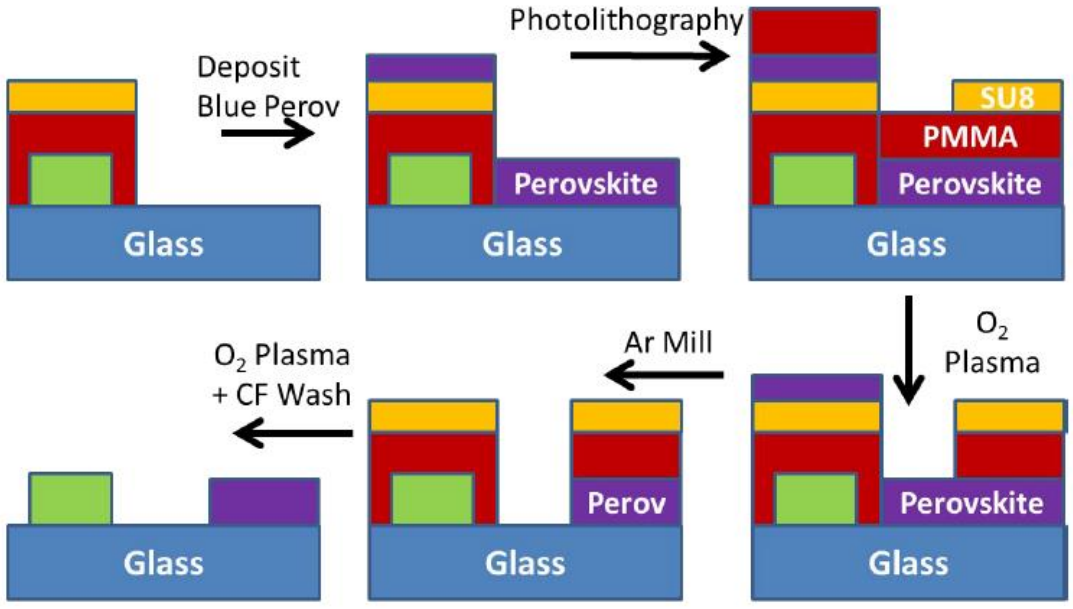

Fig. 10: Multicolor arrays are made possible by the lithography technique. Keep in mind that PMMA must be used to protect the original green perovskite film's side walls.

Compound	K Measurement technique	Size (mm)	K [W/mk]	S [μV/K]	ZT	Ref.	Growth Method
MAPbI3		10*10*8				66	STL method
MAPbI3	Steady-State Method		0.5SC 0.3SC			67	
MAPbI3		12*12*8				68	STL method
MAPbI3	MD		5.9 tetragonal			69	
MAPbI3	Laser flash		0.32-0.42 SC	920		70	
MAPbI3	3w technique		0.32 PC	-6500		71	
MAPbI3	LAaer Flash		0.38 PC	-1350		72	
MAPbI3	Laser Flash		0.36 PC			73	
MAPbI3		71*54*39				74-75	
MASnI3	Steady State Method		0.09 PC	-720	0.13	76	

A significant amount of study is now being done on lead halide perovskite because of their significant optoelectronic and photovoltaic capabilities. [77-83]. If stability and toxicity problems are resolved, these perovskites NCs might theoretically be used in light emitting devices and as labeling agents. However, applications in solar cells generally need organic free perovskite films in order to achieve electrical conductivity [84-85]. According to recent research, organic molecules can be used to cross-link the crystal grains in bulk perovskites films, improving the durability of the films. [86-87].

References:

E.R. Dohner, E.T. Hke, H.I. Karunadasa, Self-assembly of broadband white-lightemitters, J. Am.Chem. Soc. 136 (2014) 1718–1721.

E.T. McClure, M.R. Ball, W. Wind, P.M. Woodward, Cs2AgBiX6 (X=Br, Cl): Newvisible light absorbing, lead-free halide perovskite semiconductors, Chem. Mater.28 (2016) 1348–1354.

D. Cortecchia, H.A. Dewi, J. Yin, A. Bruno, S. Chen, T. Baike, P.P. Boix, M. Gratzel,S. Mhaisalkar, C. Soci, N. Mathews, Lead-free MA2CuClxBr4-x hybrid perovskites,Inorg. Chem. 55 (2016) 1044–1052.

F. Wei, Z. Deng, S. Sun, F. Zhang, D.M. Evans, G. Kieslich, S. Tominaka,M.A. Carpenter, J. Zhang, P.D. Bristowe, A.K. Cheetam, Synthesis and properties ofa lead-free hybrid double perovskite: (CH3NH3)2AgBiBr6, Chem. Mater. 29 (2017)1089–1094.

G. Volonakis, A.A. Haghighirad, R.L. Milot, W.H. Sio, M.R. Filip, B. Wenger,M.B. Johnston, L.M. Herz, H.J. Snaith, F. Giustino, Cs2InAgCl6: a new lead-freehalide double perovskite with direct band gap, J. Phys. Chem. Lett. 8 (2017)772–778.

F. Zheng, D. Saldana-Greco, S. Liu, A.M. Rappe, Material innovation in advancingorganometal halide perovskite functionality, J. Phys. Chem. Lett. 6 (2015)4862–4872.

A.K. Chilvery, A.K. Batra, B. Yang, K. Xiao, P. Guggilla, M.D. Aggarwal, R. Surabhi,R.B. Lal, J.R. Currie, B.G. Penn, Perovskites: transforming photovoltaics, a minireview"J. Photon, Energy 5 (057402) (2015) 1–14.

G. Niu, X. Guo, L. Wang, Review of recent progress in chemical stability of perovskitesolar cells, J. Mater. Chem. A 3 (2015) 8970–8980.

Y. Zhao, K. Zhu, Organic-inorganic hybrid lead halide perovskites for optoelectronicand electronic applications, Chem. Soc. Rev. 45 (2016) 655–689.

G. Kieslich, S. Sun, A.K. Cheetham, An extended tolerance factor approach fororganic-inorganic perovskites, Chem. Sci. 6 (2015) 3430–3433.

W. Travis, E.N.K. Glover, H. Bronstein, D.O. Scanlon, R.G. Palgrave, On the applicationof the tolerance factor to inorganic and hybrid halide perovskites: a revisedsystem, Chem. Sci. 7 016) 4548–4556.

E.R. Dohner, A. Jaffe, L.R. Bradshaw, H.I. Karunadasa, Intrinsic white-lightemission from layered hybrid perovskite, J. Am. Chem. Soc. 136 (2014)13154–13157.

X. Liu, L. Niu, C. Wu, C. Cong, H. Wang, Q. Zeng, H. He, Q. Fu, W. Fu, T. Yu, C. Jin,Z. Liu, T.C. Sum, Periodic organic-inorganic halide perovskite microplatelet arrayson silicon substrates for room-temperature lasing, Adv. Mater. 3 (1-9) (2016)1600137.

Z. Gu, K. Wang, W. Sun, J. Li, S. Liu, Q. Song, S. Xiao, Two-photon pumpedCH3NH3PbBr3 perovskite microwire lasers, Adv. Opt. Mater. 4 (2016) 472–479.

S. Gonzalez-carrero, R.E. Galian, J. Perez-prieto,Organometal halide perovskites bulk low-dimension materials and nanoparticles, Particle Particle Syst. Charact. 32 (2015) 709–720.

Russo N, Palmisano P, Fino D. Pd substitution effects on perovskite catalyst activity for methane emission control. Chemical Engineering Journal. 2009; 154:137–145. DOI: 10.1016/j.cej.2009.05.015.

Alifanti M, Auer R, Kirchnerova J, Thyrion F, Grange P, Delmon B. Activity in methane combustion and sensitivity to sulfur poisoning of $La_{1-x}Ce_xMn_{1-y}Co_yO_3$ perovskite oxides. Applied Catalysis, B. 2003;41:71–81. DOI: 10.1016/S0926-3373(02)00194-7.

Sora IN, Caronna T, Fontana F, FernàndezCdJ, Caneschi A, Green M. Crystal structures and magnetic properties of strontium and copper doped lanthanum ferrites. Journal of Solid-State Chemistry. 2012; 191:33–39. DOI: 10.1016/j.jssc.2012.02.020.

Klein-Kedem, N., Cahen, D. and Hodes, G., 2016. Effects of light and electron beam irradiation on halide perovskites and their solar cells. *Accounts of chemical research*, *49*(2), pp.347-354.

Gao, Y. S.; Huang, C.; Hao, C. L.; Sun, S.; Zhang, L.; Zhang, C.; Duan, Z. H.; Wang, K. Y.; Jin, Z. W.; Zhang, N.; Kildishev, A. V.; Qiu, C. W.; Song, Q. H.; Xiao, S. M., Lead Halide Perovskite Nanostructures for Dynamic Color Display. Acs Nano 2018, 12, 8847-8854.

Stoumpos CC, Malliakas CD, Kanatzidis MG. Semiconducting tin and lead iodide perovskites with organic cations: phase transitions, high mobilities, and near-infrared. photoluminescent properties. InorgChem, 2013, 52: 9019–9038

A. Pisoni, J. Jacimovic, O. S. Barisic, M. Spina, R. Gaal, L. Forro, E. Horvath, J. Phys. Chem. Lett. 2014, 5, 2488.

T. Ye, X. Z. Wang, X. Q. Li, A. Q. Yan, S. Ramakrishna, J. W. Xu, J. Mater. Chem. C 2017, 5, 1255.

M. A. Haque, M. I. Nugraha, S. H. K. Paleti, D. Baran, J. Phys. Chem 2019, 123, 14928.

X. Long, Z. Pan, Z. Zhang, J. J. Urban, H. Wang, Appl. Phys. Lett. 2019, 115, 072104.

H. Ma, C. Li, Y. Ma, H. Wang, Z. W. Rouse, Z. Zhang, C. Slebodnick, A. Alatas, S. P. Baker, J. J. Urban, Z. Tian, Phys. Rev. Lett. 2019, 123, 155901.

Saidaminov MI, Abdelhady AL, Murali B, et al. High-quality bulk hybrid perovskite single crystals within minutes by inverse temperature crystallization. Nat Commun, 2015, 6: 7586–7592

Liu Y, Yang Z, Cui D, et al. Two-inch-sized perovskite CH3NH3PbX3 (X = Cl, Br, I) crystals: growth and characterization. Adv Mater, 2015, 27: 5176–5183.

X. Mettan, R. Pisoni, P. Matus, A. Pisoni, J. Ja´cimovi´c, B. Nafradi, M. Spina, D. Pavuna, L. Forro, E. Horvath, J. Phys. Chem. C 2015, 119, 11506.

Yakunin, S.; Sytnyk, M.; Kriegner, D.; Shrestha, S.; Richter, M.; Matt, G. J.; Azimi, H.; Brabec, C. J.; Stangl, J.; Kovalenko, M. V. et al. Detection of X-Ray Photons by Solution-Processed Lead Halide Perovskites. Nat. Photon. 2015, 9, 444-449.

Green, M. A.; Ho-Baillie, A.; Snaith, H. J. The Emergence of Perovskite Solar Cells. Nat. Photon. 2014, 8, 506-514.

Liu, M.; Johnston, M. B.; Snaith, H. J. Efficient Planar Heterojunction Perovskite Solar Cells by Vapour Deposition. Nature 2013, 501, 395-398.

Nevena Marinova, W. T., Robin Humphry-Baker, M. Ibrahim Dar, Vladimir Bojinov, Shaik Mohammed Zakeeruddin, Mohammad Khaja Nazeeruddin, and Michael Gratzel Light Harvesting and Charge Recombination in CH3NH3PbI3 Perovskite Solar Cells Studied by Hole Transport Layer Thickness Variation. ACS Nano 2015, 9, 4200-4209.

Leguy, A. M.; Frost, J. M.; McMahon, A. P.; Sakai, V. G.; Kochelmann, W.; Law, C.; Li, X.; Foglia, F.; Walsh, A.; O'Regan, B. C. et al. The Dynamics of Methylammonium Ions in Hybrid Organic-Inorganic Perovskite Solar Cells. Nat. Commun. 2015, 6, 7124.

Lee, M. M.; Teuscher, J.; Miyasaka, T.; Murakami, T. N.; Snaith, H. J. Efficient Hybrid Solar Cells Based on Meso-Superstructured Organometal Halide Perovskites. Science 2012, 338, 643-647.

Anaya, M.; Lozano, G.; Calvo, M. E.; Zhang, W.; Johnston, M. B.; Snaith, H. J.; Miguez, H. Optical Description of Mesostructured Organic-Inorganic Halide Perovskite Solar Cells. J. Phys. Chem. Lett. 2015, 6, 48-53.

Tomas Leijtens, E. T. H., Giulia Grancini, Daniel J. Slotcavage, Giles E. Eperon, James M. Ball, Michele De Bastiani, Andrea R. Bowring, Nicola Martino, Konrad Wojciechowski, Michael D. McGehee, Henry J. Snaith, Annamaria Petrozza Mapping Electric Field – Induced Switchable Poling and Structural Degradation in Hybrid Lead Halide Perovskite Thin Films. Adv. Energy Mater. 2015, doi:10.1002/aenm.201500962.

Leijtens, T.; Lauber, B.; Eperon, G. E.; Stranks, S. D.; Snaith, H. J. The Importance of Perovskite Pore Filling in Organometal Mixed Halide Sensitized Tio2-Based Solar Cells. J. Phys. Chem. Lett. 2014, 5, 1096-1102.

Sun, L. Perovskite Solar Cells: Crystal Crosslinking. Nat. Chem. 2015, 7, 684-685.

Li, X.; Ibrahim Dar, M.; Yi, C.; Luo, J.; Tschumi, M.; Zakeeruddin, S. M.; Nazeeruddin, M. K.; Han, H.; Gratzel, M. Improved Performance and Stability of Perovskite Solar Cells by Crystal Crosslinking with Alkylphosphonic Acid Omega-Ammonium Chlorides. Nat. Chem. 2015, 7, 703-711.